

THE UNIVERSITY of EDINBURGH

Edinburgh Research Explorer

Co-treatment of acid mine drainage and municipal wastewater effluents: Emphasis on the fate and partitioning of chemical contaminants

Citation for published version:
Masindi, V, Foteinis, S & Chatzisymeon, E 2022, 'Co-treatment of acid mine drainage and municipal wastewater effluents: Emphasis on the fate and partitioning of chemical contaminants', *Journal of Hazardous Materials*, vol. 421, 126677. https://doi.org/10.1016/j.jhazmat.2021.126677

Digital Object Identifier (DOI):
10.1016/j.jhazmat.2021.126677

Link:
Link to publication record in Edinburgh Research Explorer

Document Version:
Peer reviewed version

Published In:
Journal of Hazardous Materials

General rights
Copyright for the publications made accessible via the Edinburgh Research Explorer is retained by the author(s) and / or other copyright owners and it is a condition of accessing these publications that users recognise and abide by the legal requirements associated with these rights.

Take down policy
The University of Edinburgh has made every reasonable effort to ensure that Edinburgh Research Explorer content complies with UK legislation. If you believe that the public display of this file breaches copyright please contact openaccess@ed.ac.uk providing details, and we will remove access to the work immediately and investigate your claim.



Download date: 07. Nov. 2026

Co-treatment of acid mine drainage and municipal wastewater effluents: Emphasis on the fate and partitioning of chemical contaminants.

V Masindi[1,&2*], S Foteinis[3], E Chatzisymeon[3]

[1]Magalies Water, Scientific Services, Research & Development Division, Erf 3475, Stoffberg street, Brits, 0250, tel: 0123816602.

[2]Department of Environmental Sciences, College of Agriculture and Environmental Sciences, University of South Africa (UNISA), P. O. Box 392, Florida, 1710, South Africa.

[3]School of Engineering, Institute for Infrastructure and Environment, University of Edinburgh, Edinburgh EH9 3JL, United Kingdom.

Abstract

The co-management of different wastewater matrices can lead to synergistic effects in terms of pollutants removal. Here, real municipal wastewater (MWW) and acid mine drainage (AMD) were co-treated studies, specifically using the monothetic analysis, i.e. one-factor-at-a-time (AFAT) approach. Optimum conditions were observed to be 15 min of mixing and 1:7 AMD to MWW liquid-to-liquid ratio. An increase in pH from ≤2.5 to ≥5.5 was observed hence leading to concurrent removal of metals, sulphate, and phosphate. Key mechanisms which were governing the co-removal of contaminants were dilution, precipitation, co-precipitation, adsorption, and crystallization. Specifically, the metal content of AMD (e.g., Al, Fe, Mn, Zn) was greatly (□95%) reduced, along with the sulphate (□92%), while MWW's phosphate content was practically removed (≥99%). The fate of Al, Fe, Mn, Sulphate, and phosphate was confirmed using the product sludge. PHREEQC geochemical model predicted the formation of (oxy)-hydroxides, (oxy)-hydro-sulphates, and metals hydroxides whilst P was removed as Pb, Mn, Al,

* Corresponding Author: Vhahangwele Masindi: vhahangwelem@magalieswater.co.za; masindivhahangwele@gmail.com; +2712 381 6602

and Fe mineral phases. Ca and sulphate were removed as basanite and Pb, Fe, and Al as hydroxyl sulphate minerals. Overall, the co-treatment of real coal AMD and MWW appear to be feasible, yet not practical since exorbitant volumes of MWW are required to attain the desired quality.

Keywords: municipal wastewater, acid mine drainage, co-treatment, partitioning of contaminants; fate of contaminants; PHREEQC geochemical model.

1 Introduction

The release of untreated acid mine drainage (AMD) and conventional municipal wastewater (MWW) is a major issue of environmental concern, both in the developed and developing world. Upon discharge, these effluents rapidly alter the physicochemical properties of receiving ecosystems, in different ways, hence affecting their ability to foster life [1, 2]. Therefore, the effective management of such effluents requires robust, yet practical, solutions given the aging, inadequate, or nonexistent wastewater treatment infrastructure in the developing world [3, 4]. Specifically, AMD comprise elevated levels of different chemical species such as metals, anions, oxyanions, and metalloids (e.g., Al, Fe, Mn, As, SO_4^{2-}), while in some cases radionuclides can also be present [5]. AMD composition is greatly influenced by the type of the host mineral being weathered, during, or post, mining [1, 6]. When sulphide-bearing minerals such as arsenopyrite and pyrite get exposed to water and air, very acidic and metalliferous drainage, known as acid mine or rock drainage (AMD or ARD), is formed [7]. In active mines AMD formation is usually prevented or AMD is treated, however, in abandoned mines AMD will rise with the water level and commence to decant to the surface contaminating adjacent ecosystems and receiving water bodies [8, 9]. On exposure, chemical species contained in AMD can pose hazardous and toxic effects to aquatic and terrestrial organisms [10, 11], while mutagenic, teratogenic, and

carcinogenic effects have also been suggested [12-14]. Nonetheless, if properly treated, minerals can be recovered and water can be reclaimed [15].

On the other hand, MWW contains notable amounts of microbial contaminants, oxyanions, and nutrients [3, 16], of which, ammonia and phosphate are the elements of prime ecological concern [17, 18] due to eutrophication pressures [3]. In conventional treatment facilities ammonia is primarily removed through biological treatment (nitrification-denitrification) [19], whilst phosphate is consumed by microorganisms [20]. The produced sludge is then dewatered and a dewatering effluent rich in ammonia and phosphates is produced [21]. This dewatering effluent, or MWW rich in phosphates, can be used as an innovative avenue for AMD treatment. Specifically, the trivalent (e.g., Fe^{3+} and Al^{3+}) and divalent (e.g., Mg^{2+}, Ca^{2+}, and Mn^{2+}) ions contained in AMD have strong affinity to phosphate [22, 23], while MWW's neutral to slightly basic pH can promote the precipitation of metals contained in AMD.

To date, a limited number of studies have focused on the effective co-treatment of MWW and AMD [24-26]. In particular, Hughes and Gray [27] used activated sludge to treat AMD and for phosphates removal from MWW. Phosphates removal was linked to the high Fe and Al content of the AMD, while metals removal was link to an increase in alkalinity attributed to MWW, which in-turn promoted their precipitation. Furthermore, Strosnider, et al. [25] explored the passive co-treatment of Zn-rich AMD and raw MWW. The authors denoted the feasibility of co-treatment at a ratio of 5:1 for AMD and MWW, respectively. However, the proposed technology entailed other treatment stages, such as lime neutralisation and bio-remediation [28-30]. On a different study, Smyntek, et al. [31] successfully demonstrated the viability of anaerobic co-treatment of AMD and MWW for the removal of key pollutants from both streams. The use of AMD sludge for phosphates removal from MWW [32] or the recovery of Fe-species from AMD

[33] and their use for phosphates removal [34] has also been explored. A two-stage co-treatment process (batch mixing of AMD-MWW, followed by anaerobic biological treatment) [35] and the co-treatment by dual-chamber microbial fuel cells [24] have also been proposed.

However, as was highlighted in a recent review by Spellman, et al. [36], various research studies have dealt with AMD-MWW co-treatment, but so far no study has dealt with the solids can are contained in the product sludge and have been generated during the interaction of AMD and MWW (co-treatment process). Therefore, in this work, apart from identifying the optimal conditions for AMD-MWW co-treatment, focus in also placed in the product sludge and specifically in identifying the fate and partitioning of inorganic contaminants post the co-treatment process. The results of this work were underpinned by state-of-the-art analytical techniques, including focused ion beam (FIB) and high-resolution field emission scanning electron microscopy (HR-FE-SEM), coupled with Energy Dispersion Spectroscopy (EDS) capabilities. In addition, the advance geochemical model PH REdox EQuilibrium (PHREEQC) (in C language) was used to provide insight on the product sludge post the co-treatment process. To the authors' knowledge, this is the first study, in the design and execution, that comprehensively quantifies the fate and partitioning of chemical species post the interaction of real coal AMD and MWW.

2 Materials and methods

2.1 Sample collection

In this work, real wastewater effluents were collected, characterised, and used for batch experimental studies. Specifically, domestic wastewater was collected from a sludge dewatering stream at a municipal wastewater treatment plant in Gauteng province, South Africa.

Alternatively, raw wastewater could be used. High-density polyethylene (HDPE) closed-mouth bottles were used as the sampling containers. As soon as the effluent was collected it was placed in a cooler and then transferred to the laboratory, where it was refrigerated at 4°C. It should be mentioned that immediately after collection the wastewater dewatering effluent was passed through a Macherey-Nagel filter paper (MN 615. Ø125mm) to remove suspended solids and debris. Similarly, real coal AMD was collected from an active coal mine in Mpumalanga province, South Africa following the aforementioned procedure. Closed-mouth HDPE bottles were used as the sampling containers and similarly with the municipal wastewater dewatering effluent, AMD was passed through a Macherey-Nagel filter paper (MN 615. Ø125mm) to remove suspended solids and debris.

2.2 Characterisation of the collected effluents

The following analytical techniques were used for aqueous samples characterisation. In-situ analyses for pH and electrical conductivity (EC) were carried out using a multi-parameter probe (HANNA instrument, HI9828). Ex-situ analyses were carried out in Magalies Water Services Laboratory, Brits, North West, South Africa, (ISO/IEC 17025:2017 accredited). The electrochemical parameters (pH and EC) of the co-treated AMD-MWW effluent were measured by means of the Thermo Scientific™ Gallery™ Plus discrete analyser. Finally, inductively coupled plasma mass spectrometry (ICP-MS) (XSeries 2, Thermo Fisher Scientific coupled to CETAC ™ ASX-520 Auto sampler) was used to identify the chemical composition of both the raw AMD and MWW effluents, as well as of the co-treated effluent.

2.3 Prediction of the synthesised mineral phases

To complement the experimental results and determine the mineral phases that are more likely to be synthesised from the interaction of AMD with the MWW dewatering effluent (MWW thereafter), geochemical modelling was applied. The primary aim was to calculate the saturation indices (SIs) of the mineral phases, based on solution compositions and their respective concentrations. To this end, the geochemical model PHREEQC along with the WATEQ4F chemical speciation model were used [37]. Thenceforth, the chemical species which were more likely to precipitate were determined using the modelled SI numbers. In this case, SI values lower than unity (< -1) denote an under saturated solution, SI values equal to unity (= 1) denote a saturated solution and, lastly, SI values higher than unity (> 1) denote a supersaturated solution.

2.4 Co-treatment studies

To acquire an in-depth understanding of the factors influencing the removal of contaminants from both wastewater matrices, three main operational parameters, i.e., the liquid-to-liquid (L-L) ratio (effect of AMD to MWW volume), mixing time (effect of contact time), and temperature were examined. Ambient pH (7.37 for MWW and 2.57 for AMD) was considered for both wastewater matrices, since this will be the case for scaled up systems. Mixing was achieved by means of an overhead stirrer at 250 rpm. Specifically, the Phipps & Bird PB-900™ Series Programmable Jar Tester was used, which allows the replication of actual plant conditions and operations. To study the effect of L-L ratio, contact time, and temperature, monothetic analysis (i.e., the one-factor-at-a-time (OFAT) method) was used. Specifically, first the L-L ratiovaried, keeping the other parameters fixed to identify the optimal L-L ratio, and then a similar approach was used for contact time and temperature, as shown in **Table 1**. The effect of temperature was explored using a hot plate.

133 **Table 1:** Examined parameters and values for the co-treatment of AMD and MWW.

Number	Ratio (AMD:MWW)	Time	Initial pHs	Final pH	Temperature
Reg no.	mL:mL	Minutes	MWW:AMD	-	℃
1	300:100	15	pH 7.37 : 2.57	2.35	26
2	300:200	15	pH 7.37 : 2.57	2.38	26
3	300:300	15	pH 7.37 : 2.57	2.39	26
4	300:400	15	pH 7.37 : 2.57	2.43	26
5	300:500	15	pH 7.37 : 2.57	2.43	26
6	300:600	15	pH 7.37 : 2.57	2.5	26
7	200:700	15	pH 7.37 : 2.57	2.64	26
8	200:800	15	pH 7.37 : 2.57	2.67	26
9	200:900	15	pH 7.37 : 2.57	2.74	26
10	200:1400	15	pH 7.37 : 2.57	3.27	26
11	50:350	15	pH 7.37 : 2.57	2.98	26
12	50:450	15	pH 7.37 : 2.57	3.09	26
13	50:550	15	pH 7.37 : 2.57	3.82	26
14	50:650	15	pH 7.37 : 2.57	4.02	26
15	50:750	15	pH 7.37 : 2.57	5.1	26
16	50:750	1	pH 7.37 : 2.57	4.9	26
17	50:750	2	pH 7.37 : 2.57	5.0	26
18	50:750	5	pH 7.37 : 2.57	5.1	26
19	50:750	10	pH 7.37 : 2.57	5.1	26
20	50:750	15	pH 7.37 : 2.57	5.2	26
21	50:750	20	pH 7.37 : 2.57	5.4	26
22	50:750	30	pH 7.37 : 2.57	5.1	26
23	50:750	45	pH 7.37 : 2.57	5.2	26
24	50:750	60	pH 7.37 : 2.57	5.3	26
25	50:750	90	pH 7.37 : 2.57	5.3	26

26	50:750	15	pH 7.37 : 2.57	5	20
27	50:750	15	pH 7.37 : 2.57	5.1	25
28	50:750	15	pH 7.37 : 2.57	5	30
29	50:750	15	pH 7.37 : 2.57	5.3	35
30	50:750	15	pH 7.37 : 2.57	5.1	40
31	50:750	15	pH 7.37 : 2.57	5.1	45
32	50:750	15	pH 7.37 : 2.57	5.2	50

Specifically, the effect of the volume of each effluent was examined by considering L-L ratios (AMD: MWW) from as low as 1:15 to as high as 3:1. The effect of contact time was examined by mixing the AMD-MWW solution at time intervals from as low as 1 min to as high as 90 min. Lastly, the effect of temperature was examined by varying the temperature from 20 to 50 ℃. Experiments were performed in triplicate and results are reported as mean values.

2.5 Characterisation of the product sludge

The analytical instruments that were used to identify the elemental and mineralogical composition, along with the morphological and chemical properties and the metal functional groups of the minerals contained in the product sludge (post-treatment) are shown in **Table 2**.

Table 2: The equipment used to identify the chemical species post co-treatment.

Parameter	Equipment	Model
Morphological properties	FIB FESEM-EDS	Focused Ion Beam (FIB) combined with High Resolution Scanning Electron Microscopy (FE-SEM) coupled with Energy Dispersive Spectroscopy (EDS) capabilities. Auriga Cobra FIB-

		FE-SEM (Model: Auriga@ V05.05) FE-SEM with Oxford EDS Sputtering System, Make: Carl Zeiss, Supplier: Carl Zeiss, USA).
Functional groups	FTIR	The Fourier Transform Infrared Spectrometer (FTIR) equipped with a Perkin-Elmer Precisely Universal Attenuated Total Reflectance (ATR) sampling accessory equipped with a diamond crystal (Perkin-Elmer Spectrum 100).
Mineralogical composition	XRD	The powder X-ray diffraction patterns (XRD) were obtained from a PANalytical X'Pert Pro powder diffractometer using Cu-Kα radiation with X'Celerator detector.
Elemental composition	XRF	The Thermo Scientific™ ARL™ PERFORM'X Sequential X-Ray Fluorescence (XRF) spectrometer for advanced materials characterisation integrates bulk elemental analysis.

Of paramount importance is the high-resolution field emission scanning electron microscope (HR-FE-SEM), equipped with the cobra column focused ion beam (FIB) and energy-dispersive X-ray spectroscopy (EDS) capabilities (Carl Zeiss AURIGA® Series modular cross-beam workstation). This instrument ensured high quality results for the morphological properties of the minerals contained in the product sludge. Furthermore, the metal functional groups were ascertained using the Fourier transform infrared spectroscopy (FTIR), with attenuated total reflectance (ATR) functionality (Perkin Elmer Spectrum 100). Elemental compositions were ascertained using the XRF. First, the samples were roasted in alumina refractory crucibles at 1,000 °C to determine the Loss On Ignition (LOI). Specifically, 1 g of sample was mixed with 6 g of Lithiumteraborate flux and fused at 1,050°C to produce a stable fused glass bead. The

Thermo Fisher ARL Perform'X Sequential XRF instrument, with the Uniquant software, was used for analyses. The software can identify elements in the periodic table between Na and U, but only the elements with concentrations above the corresponding detection limits are reported. The values were normalised, to include LOI, to determine crystal water and oxidation state changes. A standard sample material was prepared and analysed in the same manner as the examined samples.

Mineralogical composition analysis was performed by means of XRD. The samples were prepared according to the standardized Panalytical back loading system, which provides nearly random distribution of the particles. They were then analysed using the PANalytical X'Pert Pro powder diffractometer, in θ–θ configuration with an X'Celerator detector, variable divergence and fixed receiving slits with Fe filtered Co-Kα radiation (λ=1.789Å). The mineralogy was determined by selecting the best–fitting pattern from the Inorganic Crystal Structure Database (ICSD) database to the measured diffraction pattern, using X'Pert High score plus software. The relative phase amounts (weight% of crystalline portion) were estimated using the Rietveld method.

The pH and EC of both raw wastewater matrices were measured using the Thermo Scientific™ Gallery™ Plus discrete analyser (for), while their chemical characteristics by means of Inductively coupled plasma mass spectrometry (ICP-MS). The identified chemical compositions (**Table 3**)were also used as inputs in the PHREEQC geochemical model.

3 Results and discussion

3.1 Raw AMD and MWW chemical characteristics

176 The physicochemical characteristics of both wastewater streams, before their co-treatment, are
177 reported in **Table 3**.

178 **Table 3:** The chemical characteristics of the raw AMD and MWW.

Parameter	**Acid mine drainage (AMD)**	**Municipal wastewater (MWW)**
Nitrite	0.23 mg/L	0 mg/L
Sulphate (SO_4^{2-})	12.42 mg/L	72 mg/L
Iron (Fe)	1.80 mg/L	0.10 mg/L
Manganese (Mn)	98.71 mg/L	0.10 mg/L
Chromium (Cr)	0.06 mg/L	0 mg/L
Copper (Cu)	0.25 mg/L	0 mg/L
Nitrite (NO_2^-)	1.30 mg/L	0.01 mg/L
Lead (Pb)	0.28 mg/L	0 mg/L
pH	2.57	7.37
Aluminium (Al)	500.00 mg/L	0.01 mg/L
Electrical conductivity (EC)	1.70 mS/cm	388 mS/cm
Ammonia (NH_3)	0.01 mg/L	120.70 mg/L
Zinc (Zn)	120.00 mg/L	0 mg/L
Phosphate (PO_4^{3-})	1.10 mg/L	114 mg/L
Calcium (Ca)	622. mg/L	27 mg/L
Magnesium (Mg)	495.00 mg/L	50 mg/L
Alkalinity	0 mg/L $CaCO_3$	813 mg/L $CaCO_3$
Chemical oxygen demand	1480 mg/L	71 mg/L

As was expected, both effluents contained elevated concentrations of different contaminants (**Table 3**). Specifically, MWW was observed to be enriched with ammonia (NH_3) and phosphate (PO_4^{3-}), containing lower concentrations of sulphate (SO_4^{2-}) and base metals (i.e., calcium (Ca) and magnesium (Mg)). Relatively high alkalinity was also observed (≥813 mg/L $CaCO_3$), rendering MWW's pH circumneutral (pH = 7.37). . Finally, the presence of PO_4^{3-} and NH_3 can be traced back to the decomposition of organic waste (mainly urea, amino acids and phospholipids) from living organisms [38], which also leads to high chemical oxygen demand (COD) values.

On the other hand, AMD was observed to comprise iron (Fe) and SO_4^{2-} as major elements, zinc (Zn), manganese (Mn), aluminium (Al), calcium (Ca), and magnesium (Mg) as intermediate elements, while lead (Pb), chromium (Cr), and copper (Cu) were also present, but as trace elements. These elements and concentrations are typical for AMD matrices, while the presence of Fe and SO_4^{2-} as major elements suggest that this AMD matrix is formed from pyrite's (FeS_2) oxidation [39, 40]. As was expected, the COD value was significantly lower than that of the MWW. The presence of Zn also implies the existence of zinc sulphide (ZnS) in the underlying mine lithology [41].

As shown in **Table 3**, the concentrations of the aforementioned elements in both wastewater matrices are well above the prescribed limits for water being discharged to the environment, as specified in different standards, guidelines, and specifications [42-44]. Therefore, the high concentrations of a vast array of different contaminants in both wastewater matrices raises the question of whether their co-treatment would enjoy synergistic effects in contaminants removal

and, if that is the case, what are the optimal co-treatment conditions (L-L ratio, contact time, and temperature).

3.2 Geochemical modelling

To predict the fate of chemical species during the co-interaction of AMD with MWW, the PHREEQC geochemical model was employ. It was found that the chemical species in the raw AMD matrix (Table 3) exist as divalent, trivalent, and oxyanions. However, different complexes are formed during the co-mixing of these wastewater effluents, with the results for the saturation indexes listed in **Table 4**.

Table 4: The chemical names, saturation index, and chemical formulas of the produced minerals from AMD-MWW co-treatment.

Chemical name	**Saturation index (SI)**	**Chemical formula**
Alunite	6.93	$KAl_3(SO_4)_2(OH)_6$
Anglesite	3.44	$PbSO_4$
Anhydrite	0.01	$CaSO_4$
Cupric Ferrite	5.04	$CuFe_2O_4$
Cuprous Ferrite	1.59	$CuFeO_2$
Epsomite	0.70	$MgSO_4{:}7H_2O$
Goethite	6.00	FeOOH
Gypsum	0.00	$CaSO_4{:}2H_2O$
Hematite	14.13	Fe_2O_3
Hxypyromorphite	0.26	$Pb_5(PO_4)_3OH$

Jarosite(ss)	15.67	$(K_{0.77}Na_{0.03}H_{0.2})Fe_3(SO_4)_2(OH)_6$
Jarosite-K	15.17	$KFe_3(SO_4)_2(OH)_6$
Jarosite-Na	11.13	$NaFe_3(SO_4)_2(OH)_6$
Jarosite-H (Hydronium)	10.64	$(H_3O)Fe_3(SO_4)_2(OH)_6$
Jurbanite	3.38	$AlOHSO_4$
Maghemite	3.73	γ-Fe_2O_3
Magnetite	8.55	Fe_3O_4
Manganese(II)hydrogen phosphate	7.67	$MnHPO_4$
Lead phosphate	2.59	$Pb_3(PO_4)_2$
Lead(II) hydrogen phosphate	2.68	$PbHPO_4$
Plumbogummite	4.65	$PbAl_3(PO_4)_2(OH)_5{:}H_2O$
Strengite	9.80	$FePO_4{:}2H_2O$

As shown in **Table 4**, the PHREEQC results further support the hypothesis that different mineral phases are more likely to be synthesized from the interaction of AMD with MWW, which will then precipitate, if the pH conditions allow, with the product sludge. Firstly, the Fe-species that can be synthesized are Goethite (FeOOH), Hematite (Fe_2O_3), Maghemite (γ-Fe_2O_3), Magnetite (Fe_3O_4), Jarosite(ss) ($(K_{0.77}Na_{0.03}H_{0.2})Fe_3(SO_4)_2(OH)_6$), Jarosite-K ($KFe_3(SO_4)_2(OH)_6$), Jarosite-Na ($NaFe_3(SO_4)_2(OH)_6$), Jarosite H ($(H_3O)Fe_3(SO_4)_2(OH)_6$), CupricFerrite ($CuFe_2O_4$), and CuprousFerrite ($CuFeO_2$). Furthermore, the Al-species that can be synthesized include Alunite ($KAl_3(SO_4)_2(OH)_6$) and Jurbanite ($AlOHSO_4$). Fe and Al also precipitated as iron (oxy)-hydroxides and aluminium (oxy)-hydroxides. Phosphates were removed as Hxypyromorphite ($Pb_5(PO_4)_3OH$), Manganese(II) hydrogen phosphate ($MnHPO_4$), Lead phosphate ($Pb_3(PO_4)_2$,), Lead(II) hydrogen phosphate ($PbHPO_4$), Plumbogummite ($PbAl_3(PO_4)_2(OH)_5{:}H_2O$), and

Strengite ($FePO_4{:}2H_2O$). Ca was removed as gypsum ($CaSO_4{\cdot}2H_2O$). Mg was removed as epsomite ($MgSO_4{:}7H_2O$). Lastly, $SO_4^{2-}$was removed as $CaSO_4{\cdot}2H_2O$and Pb, Fe, and Al hydroxyl sulphate minerals. $NH_3$was partially removed as nitrogen gas and this could have followed the Le Chatelier's principle. As a preamble, the PHREEQC results were corroborated by the ones obtained using FTIR and high-resolution SEM-EDS. Furthermore, the predicted mineral phases are in line with what has been reported elsewhere [48-50]. Therefore, it appears that different minerals are found in the product sludge, after co-treatment, which if could be recovered could possibly offset the cost and environmental impacts of the co-treatment process.

3.3 Optimisation studies

3.3.1 Effect of contact time

The results for varying the contact time are shown in **Figure 1**.

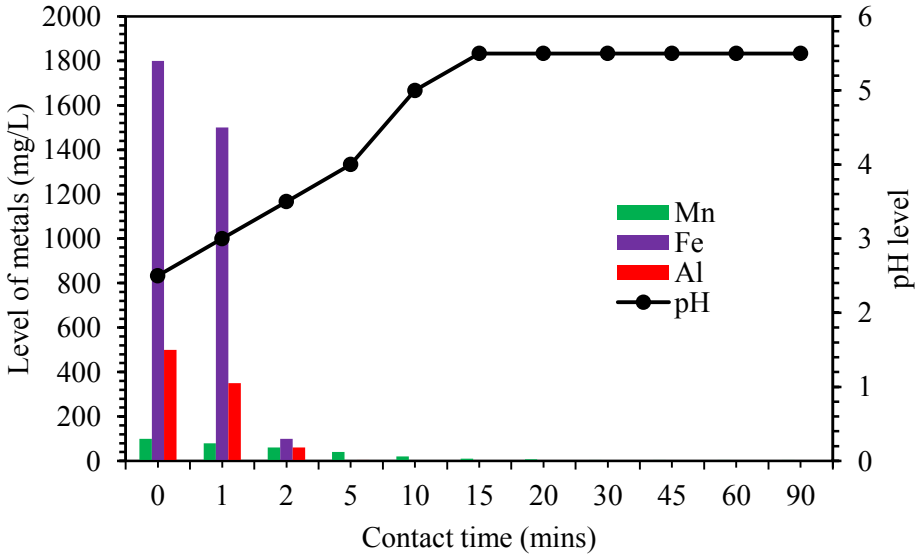


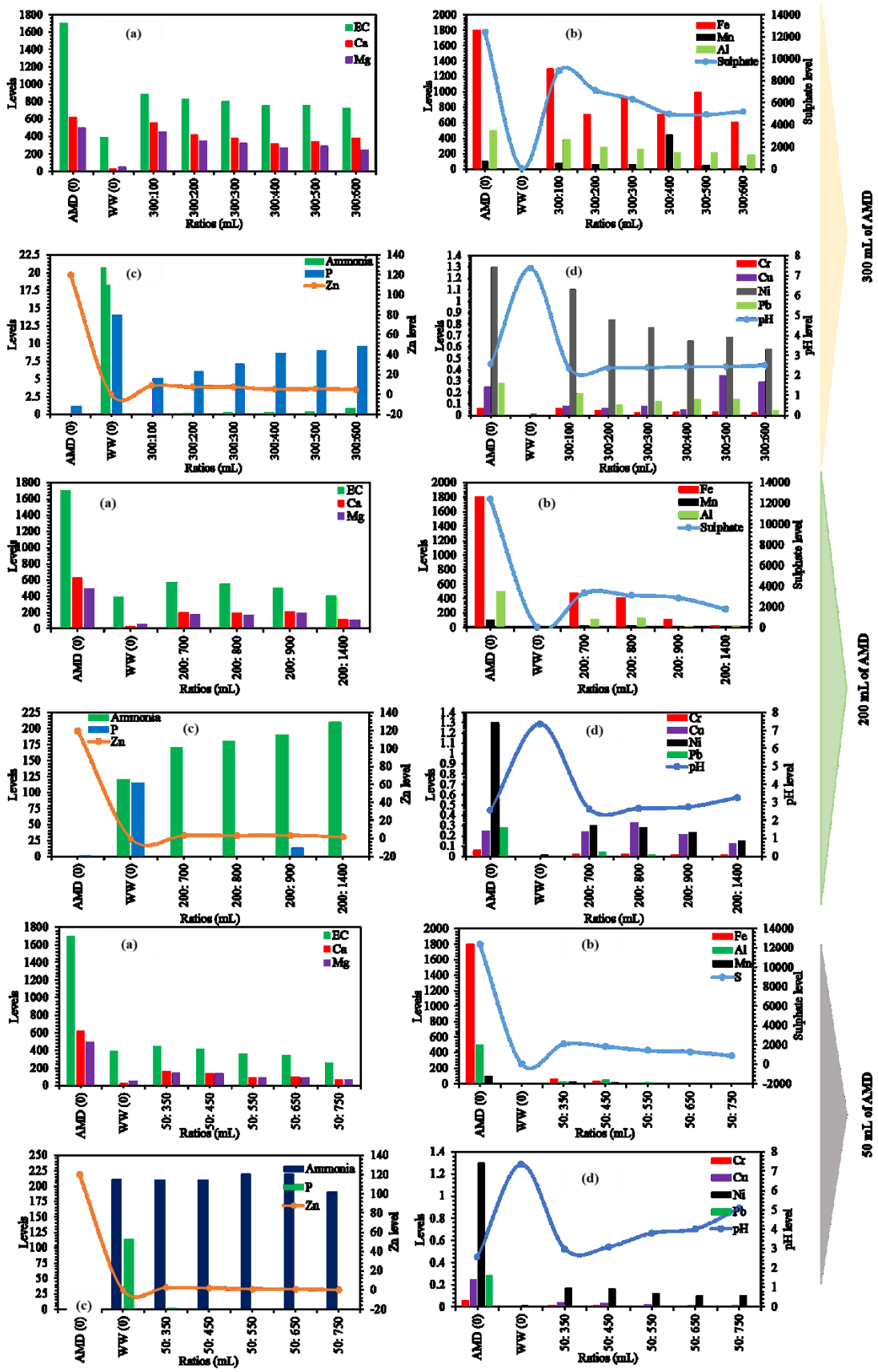
Figure 1: The influence of contact time on the removal of contaminants during the interaction of AMD with MWW (conditions: ambient temperature and pH, 50:750 L-L ratio for AMD and MWW respectively, and 250 rpm mixing speed).

As fixed parameters ambient temperature (26 ^{o}C) and pH (7.37 for MWW and 2.57 for AMD) for both effluents were considered, while the AMD to MWW (L-L) ratio was kept constant at 1:15, i.e., 50 mL of AMD were diluted in 750 mL MWW. The reason for using this high dilution value is that for the effective mineral precipitation, the pH of the AMD-MWW matrix should be >5. As shown in **Figure 1**, a decrease in contaminants levels during the interaction of AMD with MWW is observed with increasing contact time. This is attributed to co-reactions and synthesis of new products against other complexes. It should also be noted that the Fe-based minerals contained in AMD also scavenge wastewater's phosphates content, leading to its reduction, as will be discussed below. Using the pH value as an indicator, it is observed that the reaction reaches equilibrium at 15 min of mixing. However, after 5 min, the main pollutants contained in the AMD matrix, i.e., Al, Fe, and Mn, were drastically reduced, which denotes that relatively fast chemical reactions are taking place. These elements were observed to have practically depleted after 15 min of mixing and therefore the 15 min contact time, where the pH value has reached equilibrium, was considered as the optimal contact time.

3.3.2 Effect of AMD to MWW ratio

To gain insight into the processes that govern contaminants attenuation, a wide range of L-L (AMD:MWW) ratios, from as low as 1:15 to as high as 3:1, were examined using three different volumes for the AMD, i.e. 50, 200, and 300 mL, and varying the MWW volumes from 100 to

255 1400 mL (**Table 1**). The variations in the levels of different water quality determinants with
256 varying AMD-MWW ratios are shown in **Figure 2**.


(a)
EC
Ca
Mg
Levels
(b)
Fe
Mn
Al
Sulphate
Sulphate level
(c)
Ammonia
P
Zn
Zn level
(d)
Cr
Cu
Ni
Pb
pH
pH level
AMD (0)
WW (0)
300:100
300:200
300:300
300:400
300:500
300:600
200: 700
200: 800
200: 900
200: 1400
50: 350
50: 450
50: 550
50: 650
50: 750
Ratios (mL)
300 mL of AMD
200 mL of AMD
50 mL of AMD

257

Figure 2: Variations in the levels of different water quality determinants, i.e., (a) EC, Ca, and Mg; (b) Fe, Al, Mn, and sulphate; (c) ammonia, P, Zn; and (d) Cr, Cu, Ni, Pb, and pH, with varying AMD-MWW ratios (conditions: ambient temperature and pH, 250 rpm mixing speed, and 15 min contact time).

AMD dilution with MWW grossly influences the pH of the AMD-MWW matrix and by extension the ability of the co-treatment process to precipitate the metal content of AMD. The L-L ratio also influences the (co)adsorption and other chemical reactions that lead to minerals synthesis, and thus it will define the minerals that can be recovered from the product sludge. This plays a significant role in the formation of oxyhydrosulphates, amongst other chemical species. It should be noted that minerals recovery and water reclamation are important factor for introducing reuse, recycle, and resource recovery paradigms in wastewater management [15, 16, 45]. This can promote the sustainable management of such wastewater streams. Furthermore, it has been reported that significant MWW alkalinity is consumed during AMD-MWW co-treatment, implying that an alkali addition might be necessary [27]. As such, the pH could be adjusted using chemical reagents such as sodium hydroxide (NaOH) [41] and periclase (MgO) [46, 47], but chemical addition is outside the remit of this work.

The AMD-MWW matrices were mixed for 15 min, which was identified as the optimal contact time. As shown in **Figure 2**, contaminants removal efficacy largely increases with decreasing AMD: MWW L-L ratios, i.e., when AMD is diluted to larger MWW volumes. This is an indication that dilution plays an indispensable role in contaminants attenuation from both wastewater streams, and particularly from the AMD. Interestingly, the final levels, after co-treatment, of different contaminants were not proportional to the dilution factors, thus, grossly suggesting that other mechanisms, such as adsorption, are at play which aid the attenuation of

281 contaminants from the AMD-MWW matrix. This is further supported by the fact that the EC
282 value of each examined L-L ratio grossly varied from the mean EC value, suggesting the
283 existence of other mechanisms beyond dilution.

284 As shown in **Figure 2**, when the pH was ≥ 5, then □95% of the metal content (i.e., Al, Fe, Mn,
285 and Z) is removed, with the required AMD:MWW ratio to reach this pH value being 1:7, i.e., the
286 50:350 ratio. Higher dilution with MWW is not practical, since typically the AMD volumes that
287 need treatment are larger than the MWW volumes. A drastic reduction in SO_4^{2-} (>20%) was also
288 observed. Thenceforth, the PHREEQC model confirmed the synthesis of Jarosite-K and Jarosite-
289 Na and oxyhydrosulphates. The existence of Jarosite-K and Jarosite-Na is supported by the
290 levels of K and Na that were identified in the product sludge, as is discussed below.

291 Overall, an increase in AMD dilution with MWW can play a critical role in contaminants
292 attenuation, with the optimal AMD: MWW L-L ratio, in terms of real-world applications, being
293 1:7. Specifically, MWW is deficient in metals and SO_4^{2-}but it is rich in NH_3 and phosphates. On
294 the other hand, AMD is rich in metals and $SO_4^{2-}$and deficient in NH_3 and phosphate. As such,
295 phosphate affinity to divalent and trivalent Fe and Al contained in AMD, along with the increase
296 in the pH of the AMD-MWW matrix, can be considered as the underlying mechanisms for
297 contaminants removal. It should be also mentioned that no linear relationship between dilution
298 (L-L ratio) and contaminants concentrations was identified, which suggest that other mechanisms
299 such as precipitation, adsorption, co-precipitation, co-adsorption are contributing to the
300 attenuation of chemical species in the AMD-MWW matrix.

301 **3.3.1 Effect of temperature**

Finally, the effect of temperature on the co-treatment of AMD and MWW was examined and results are shown in **Figure 3**.

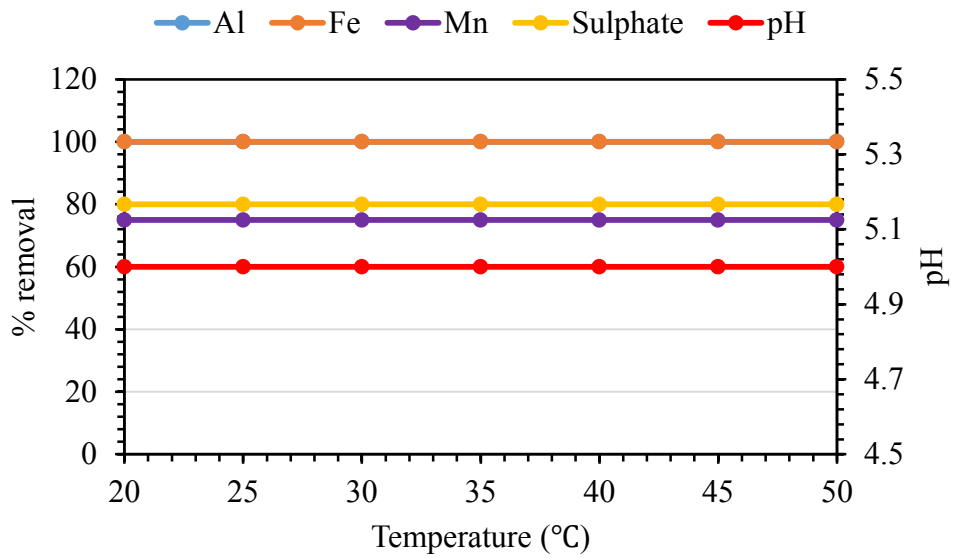


Figure 3: The effect of temperature variation on the co-treatment of AMD and MWW (conditions: ambient pH, 50:750 L-L ratio for AMD and MWW respectively, 15 min contact time, and 250 rpm mixing speed).

As shown in **Figure 3**, the effect of temperature (examined range 20 ℃ to 50 ℃) on the removal of contaminants from the two wastewater streams is insignificant. Specifically, the removal efficacies for Al, Fe, Mn, SO_4^{2-}, and pH, as expressed in % removal, were observed to remain constant regardless of temperature variations (**Figure 3**).In all examined cases ≥97% of Al and ≥99% of Fe were removed from AMD post the co-treatment, regardless the changes in the temperature of the AMD-MWW matrix, i.e., from 20 ℃ to 50 ℃. This is also the case for $SO_4^{2-}$and Mn, where the removal percentages were practically constant (80% and 75% respectively) and were not affected by temperature variations. However, even though temperature appears to not affect most of the main pollutants of both AMD and MWW effluents,

317 increased temperatures can promote the removal of NH_3 as nitrogen gas [2]. Overall, the
318 removal efficiencies of some of the main contaminants appear to be unaffected by temperature
319 variations. Therefore, given the engineering challenges of wastewater temperature control at
320 industrial scale, this technology is most likely to be scaled up under the South African and other
321 sub-Saharan countries temperate climate.

322 **3.4 Co-treatment of AMD and MWW at optimal conditions**

323 Here the contaminant removal efficacies under the identified optimal conditions , i.e., L-L ratio
324 1:7 (AMD: MWW), contact time 15 min, and ambient water temperature, are reported (**Table 5**)
325 and discussed. .

326 **Table 5:** The effect of co-treating AMD-MWW at 1:7 ratio, 15 min contact time, and ambient
327 temperature.

Determinant	AMD	MWW	Co-treatment	Theoretical product
pH	2.57	7.37	5.1	4.97
SO_4 (mg/L)	12418	72	900	12490
Fe (mg/L)	1800	0.09	0.90	1800.09
Mn (mg/L)	98,71	0.09	6.90	98.8
Cr (mg/L)	0.06	0	0.03	0.06
Cu (mg/L)	0.25	0	0.01	0.25
Ni (mg/L)	1.30	0.01	0.10	1.31
Pb (mg/L)	0.28	0	0	0.28
Al (mg/L)	500	0,01	0,20	500

EC (mS/cm)	1700	388	256	2088
NH_3 (mg/L)	<0.01	210.70	190	210.71
Zn (mg/L)	120	<0.02	0.10	120.02
PO_4 (mg/L)	1.10	140	1.26	141.1
Ca (mg/L)	622	27	66	649
Mg (mg/L)	495	50	71	545
Alkalinity	0 mg/L $CaCO_3$	813 mg/L $CaCO_3$	250	406.5
COD	1480 mg/L	71 mg/L	1250	775.5

As shown in **Table 5**, MWW was rich in NH_3 and phosphates, while of other chemical species, such as Mg and Ca which also are partly responsible for the elevated EC value, were present. Similar to the pH of natural water, the pH of MWW was circumneutral. Overall, the identified concentrations can be considered typical for MWW [25, 30, 49]. On the other hand, the AMD was rich in Al, Fe, and SO_4^{2-}, while low concentrations of Mn, Mg, Ca, and heavy metals were also identified. The pH was acidic, which causes the dissolution of the identified metals in its matrix.

Post co-treatment, the product water was observed to comprise different concentrations of contaminants from both streams, however, at significantly lower concentrations, suggesting that synergistic effects are achieved during co-treatment. Specifically, contaminants metals precipitate in the product sludge due to the increase in pH. The reduction of NH_3 concertation (~10%) and this may be attributed to co-adsorption and co-precipitation and to ammonia stripping. The drastic reduction of phosphates could be explained by Al and Fe scavenging and their subsequent precipitation in the product sludge, as shown in equations (1) and (2) [23]:

342 $Al^{3+} + PO_4^{3-} \rightarrow AlPO_4$ (1)

343 $Fe^{3+} + PO_4^{3-} \rightarrow FePO_4$ (2)

344

345 As a result the product sludge was found to contain valuable minerals, as is discussed in detail
346 below, and therefore their recovery could promote resource recovery paradigms in wastewater
347 management.

348 Overall, it appears that AMD-MWW co-treatment can be promising, however based on the
349 obtained results (**Table 5**) cannot act as a standalone treatment method. At best, AMD-MWW
350 co-treatment can be considered as a low-cost pre-treatment method, albeit bearing in mind that
351 much larger MWW compared to the AMD volume will be required in real-word applications.
352 Nonetheless, as mentioned above the co-treatment process can be modified using chemical
353 addition, such as sodium hydroxide (NaOH), to control the pH of the AMD-MWW effluent.
354 Furthermore, the high ferrous content in the AMD matrix suggest that this can be utilized for
355 mineralizing organic compounds, mainly found in the MWW matrix, using the Fenton's reagent,
356 an advance oxidation process (AOPs) where hydrogen peroxide (H_2O_2) and ferrous iron catalyst
357 are used for decontamination [51]. For example, Fe^{2+} -rich AMD [52] or iron recovered from
358 AMD sludge can be use as the catalyst in Fenton reagent [53]. The Fenton's reagent can also be
359 assisted by ultraviolet (UV)/visible irradiation, i.e., photo-Fenton, thus further improving the
360 removal of micro-contaminants and organic pollutants that are typically contained in MWW
361 [51]. By improving treatment efficiency apart from minerals recovery, water could also be
362 reclaimed (e.g., for irrigation), which would be of paramount importance in reuse, recycle, and

363 resource recovery wastewater management schemes. All the above will be examined in future
364 works of our group.

365 ### 3.5 Characterisation of the minerals contained in product sludge

366 #### 3.5.1 Elemental composition analysis using XRF

367 The elemental composition (Wt%) of the product sludge, i.e., after AMD-MWW co-treatment, ,
368 was identified using the XRF technique. To verify the obtained data, the United States
369 Geological Survey (USGS) Standard Reference Material BHV O-1 was used. Results for the
370 BHV O-1 standard and for the product sludge are shown in **Table 6.**

371 **Table 6:** Elemental composition (Wt%) of the product sludge.

Composition (Wt%)	**BHV O-1 Certified standard**	**BHV O-1 Analysed**	**Product sludge**
SiO_2	49.94	48.65	0.80
Al_2O_3	13.8	13.83	2.53
MgO	7.23	7.66	2.37
Na_2O	2.26	1.90	0.89
P_2O_5	0.273	0.33	15.93
Fe_2O_3	12.23	11.86	27.31
K_2O	0.52	0.53	1.02
CaO	11.4	10.62	1.34
TiO_2	2.71	2.49	0.01
V_2O_5	0.0566	0.06	0,01

Cr_2O_3	0.0422	0.04	0,01
MnO	0.168	0.17	0.22
NiO	0.0154	0.02	0.01
CuO	0.017	0.02	0.00
ZrO_2	0.0242	0.10	0.01
S	-	0.02	0.66
Cl	-	0.01	0.01
Co_3O_4	-	0.01	0.03
ZnO	-	0.02	0.03
Ag_2O	-	0.04	0.05
SrO	-	0.12	0,01
Y_2O_3	-	0.02	0.01
Nb_2O_5	-	0.04	0.01
WO_3	-	0,01	0.01
PtO_2	-	0.01	0.01
ThO_2	-	0.05	0.02
Loss of ignition (LOI)	-	1.37	46.73
Total	100.69	**99.99**	**99.98**

As shown in **Table 6**, the product sludge was dominated by Fe and P as major elements, amongst intermediate concentrations of Mg, Al, Ca, S, and K, and traces of other elements. This confirms that the interaction of AMD with MWW can lead to the removal of contaminants from both wastewater streams and their settling in the product sludge. The high LOI values that were

observed in the product sludge denote the presence of hydrated species in the formed sludge, as is also reported in the XRD and FTIR results and was further conformed by PHREEQC model.

3.5.2 Mineralogical composition using XRD

The mineralogical properties of mineral phases that were contained in the product sludge were measured by means of XRD and the obtained XRD pattern is shown in **Figure 4**.

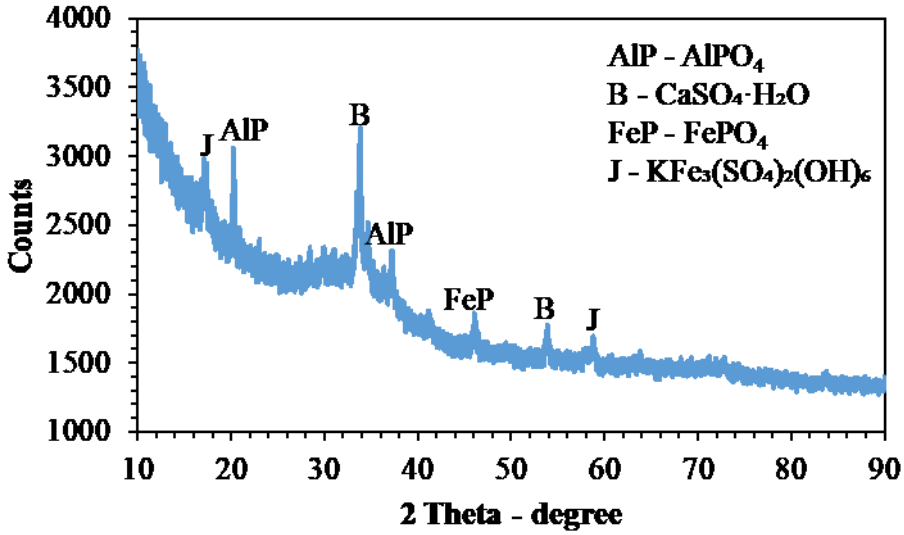


Figure 4: Mineral phases contained in the product sludge.

As shown in **Figure 4**, the interaction of AMD with the MWW led to the formation of crystalline and amorphous phases. The crystalline phases were observed for basanite ($2CaSO_4 \cdot H_2O$), aluminium phosphate ($AlPO_4$), iron phosphate ($FePO_4$), and jarosite-K ($KFe_3(SO_4)_2(OH)_6$). The results corroborate the ones obtained from the PHREEQC geochemical model. The results are also in agreement with the ones obtained by the XRF and particularly on the key elements which were observed to be prominent in the XRF analysis. The XRD results further support the hypothesis that Fe and SO_4^{2-} from the AMD matrix, and K and P from the MWW matrix co-

precipitate from their initial matrices to the product sludge to form the observed mineral phases (**Figure 4**). The noise in the peak confirms that a large fraction of the formed minerals phases that is not crystalline, due to formation conditions.

3.5.1 Metal functional groups of the product sludge

The metal functional groups of the minerals that were synthesized during the co-treatment process and precipitated in the product sludge were identified and characterised using Fourier transform infrared (FTIR) spectroscopy. In **Figure 5**, the FTIR spectrum, along with the metal functional groups that were identified in the product sludge, are shown.

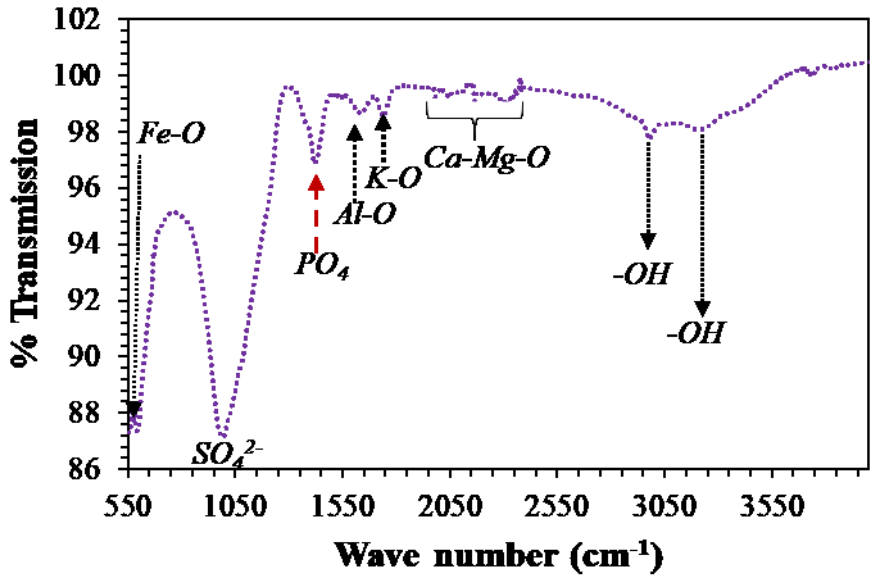


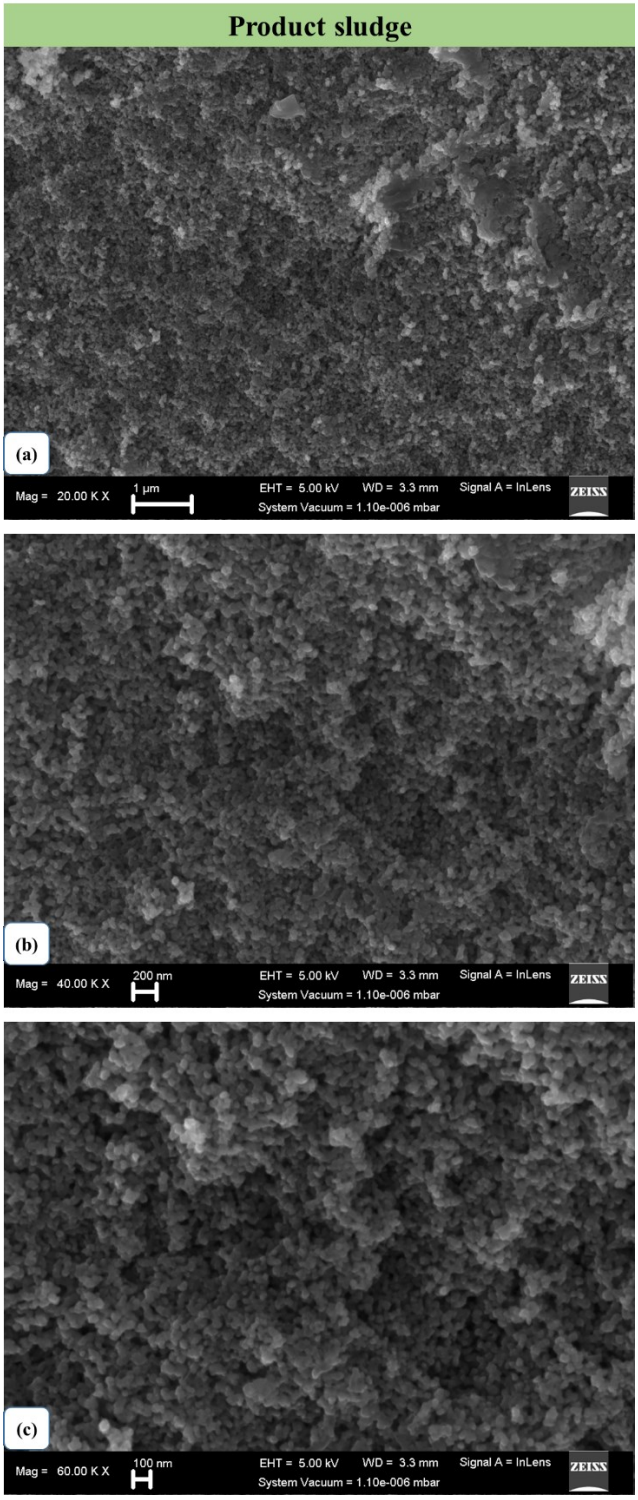
Figure 5: The metal functional groups that were identified in the product sludge using FTIR technique.

Firstly, FTIR spectroscopy revealed the presence of Fe-O (550 cm^{-1}) [54] in the product sludge. This implies the existence of Fe-based minerals in the sludge, which confirms the ability of the co-treatment method to remove Fe-species that were initially contained in the AMD matrix.

Furthermore, the presence of Al-O (600-700, and 1550 cm^{-1}) and SO_4 (1050 cm^{-1}) [7] further denotes the attenuation of these elements from the AMD matrix and their transition to the product sludge. Ca-Mg-O groups (…. cm^{-1}) [55] denote the presence of base metals, which are an indication that these metals attenuate P through co-adsorption and co-precipitation. Furthermore, FTIR spectroscopy also revealed the presence of P and K, which are the key elements in human waste. Their presence confirms that these chemical species have precipitated from the MWW matrix to the product sludge. The presence of water (-OH group) denotes that the product sludge is hydrated, and the mineral phases therein are in hydrated form and nature (hydroxides). The obtained results are in agreement with the PHREEQC results. . It should be noted that due to competing ions and multiple interferences, struvite could not be formed from this co-treatment process. Results are in agreement with the ones presented in the water quality section and with the FE-SEM-EDS results, which are shown below.

3.5.2 Morphological properties of the synthesised minerals

The morphological characteristics of the productτ sludge are shown in **Figure 6**. As detailed in **Table 2**, FIB combined with high resolution (HR) FE-SEM and coupled with EDS was used to identify the morphological properties of the synthesised minerals. In particular, the Auriga Cobra modular cross-beam workstation was used. The FE-SEM function offers clear, ultra-high-resolution images, with practically no distortion (**Figure 6**). This ensures that the obtained images can be used towards effectively revealing the morphology of the minerals under study.



423

424 **Figure 6 (a-c):** The FE-SEM images showing the changes in morphological properties of the
425 resultant sludge from the co-treatment of AMD and MWW at (a)1 µm, (b) 200 nm, and (c) 100
426 nm magnification.

As shown in **Figure 6**, the product sludge comprise regular shaped spherical-like structures, homogenously distributed across its entire surface. Furthermore, the morphological properties of the sludge surface were observed to remain the same regardless of the magnification (from 1 µm to 100 nm), hence denoting uniformity and consistency in the obtained results. The FE-SEM results also suggest that the sludge comprise nanomaterials with octagonal structures. The octagonal structure has been widely reported for Fe-based minerals, such as goethite and magnetite [56]. Therefore, the presence of octagonal and spherical particles could further allude to the presence of Fe-based minerals. The observed uniformity also suggests that these minerals are well-synthesized and cohesive. This is further confirmed by the elemental mapping and spot-point-shoot results, which are discussed below.

3.5.3 Elemental composition of the synthesised minerals

As mentioned above, the utilised FE-SEM instrument was equipped with an Energy-dispersive X-ray spectroscopy (EDS) detector, which was used towards identifying the map sum spectrum and elemental composition of the product sludge. Results are shown in **Figure 7**.

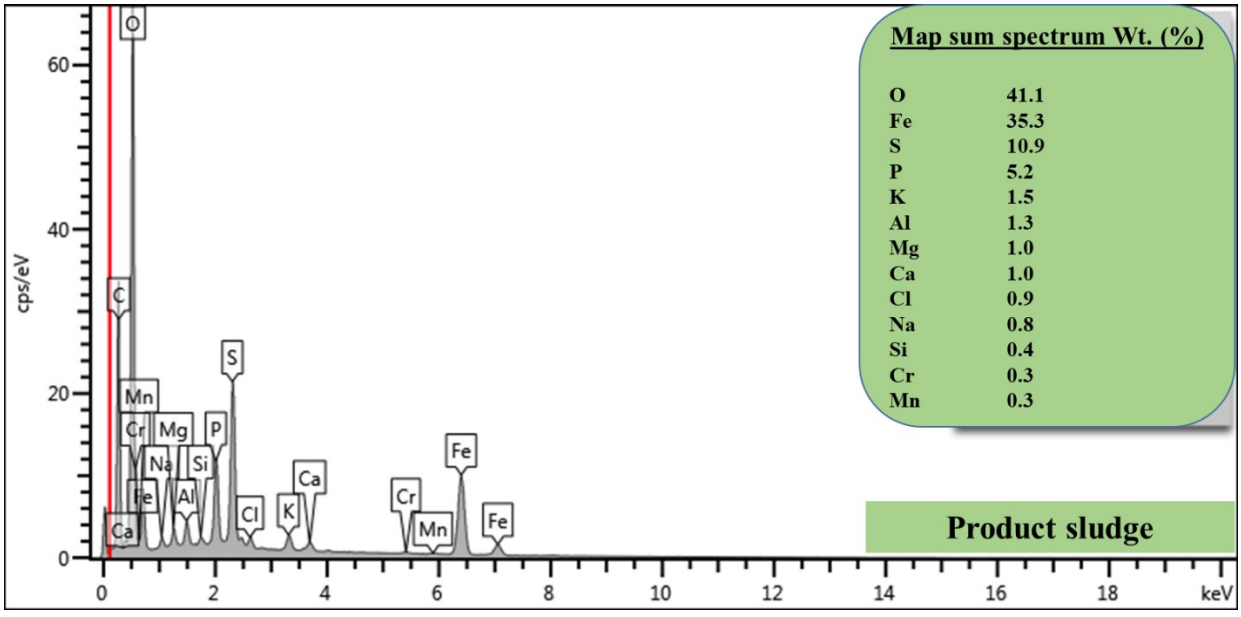
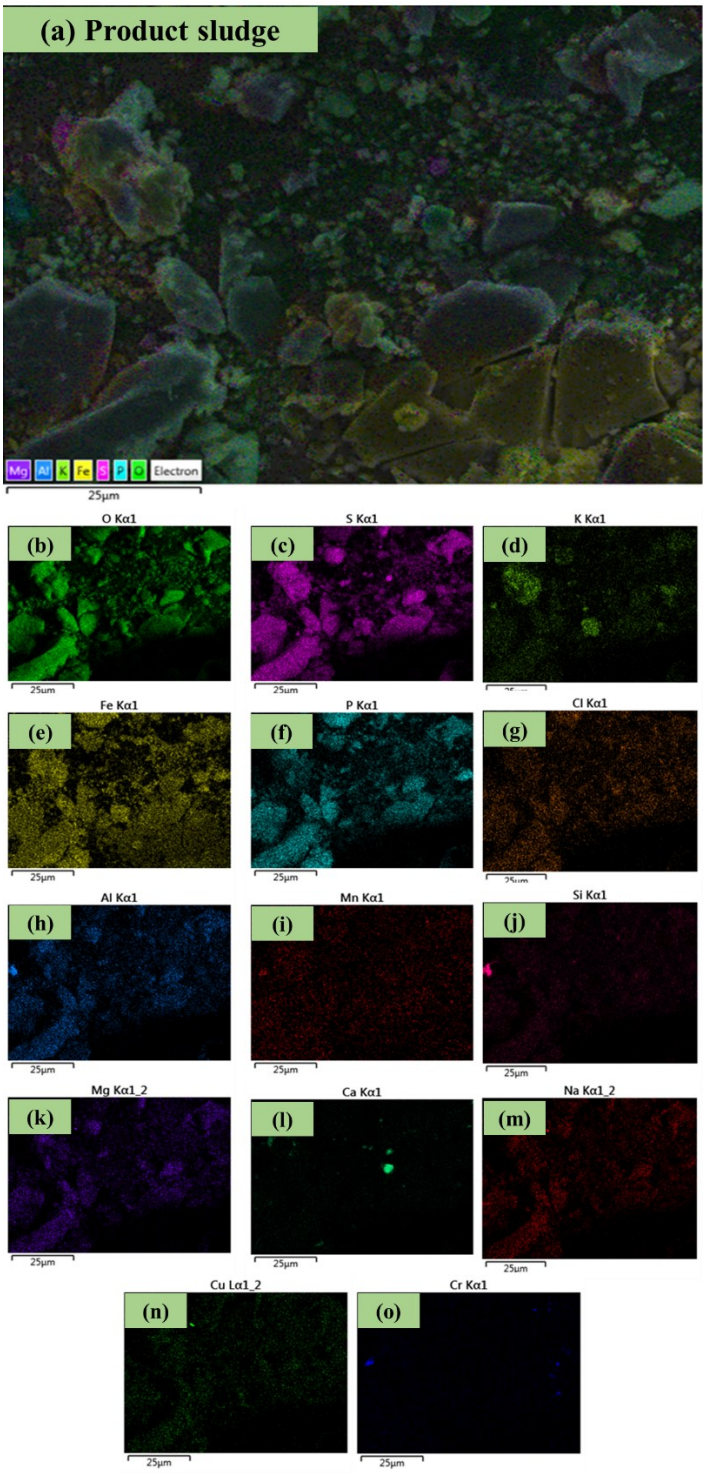


Figure 7: The map sum spectrum showing the elemental composition of the product sludge.

As shown in **Figure 7**, the product sludge was found to comprise O, Fe, S and P as its major elements, whilst low concentrations of K, Al, Mg, and Ca and traces of Na, Si, Cr and Mn were also identified. This composition denotes a clear representation of the AMD-MWW mixture in the product sludge and by extension the attenuation of these contaminants from the AMD-MWW matrix and their settling to the product sludge. Furthermore, as discussed above, Mg contributes to the removal of NH_4^+ and PO_4^{3-} from AMD-MWW matrix, while Fe and Al were removed as oxyhydrosulphates, as was emphasized in the PHREEQC results. The sorption of P onto Fe and Al trivalent and Mn, Ca, and Mg divalent ions is also apparent due to affinity ranges. Thenceforth, the formation of oxy-hydroxides and oxy-hydrosulphates are apparent in the obtained sum spectrum results (**Figure 7**). Furthermore, the presence of K is traced back to the jarosite species. As a result, the sludge appears to be rich in minerals that could be possibly harvested for future beneficiation. This could offset the cost and environmental impacts of the co-treatment process and promote resource recovery paradigms in wastewater management.

3.5.4 Elemental composition analysis

In this section, the FE-SEM and the corresponding EDS elemental mapping images of the product sludge are given and discussed. The aim is to acquire an in-depth understanding of the sludge's elemental composition. Results are shown in **Figure 8**.



462

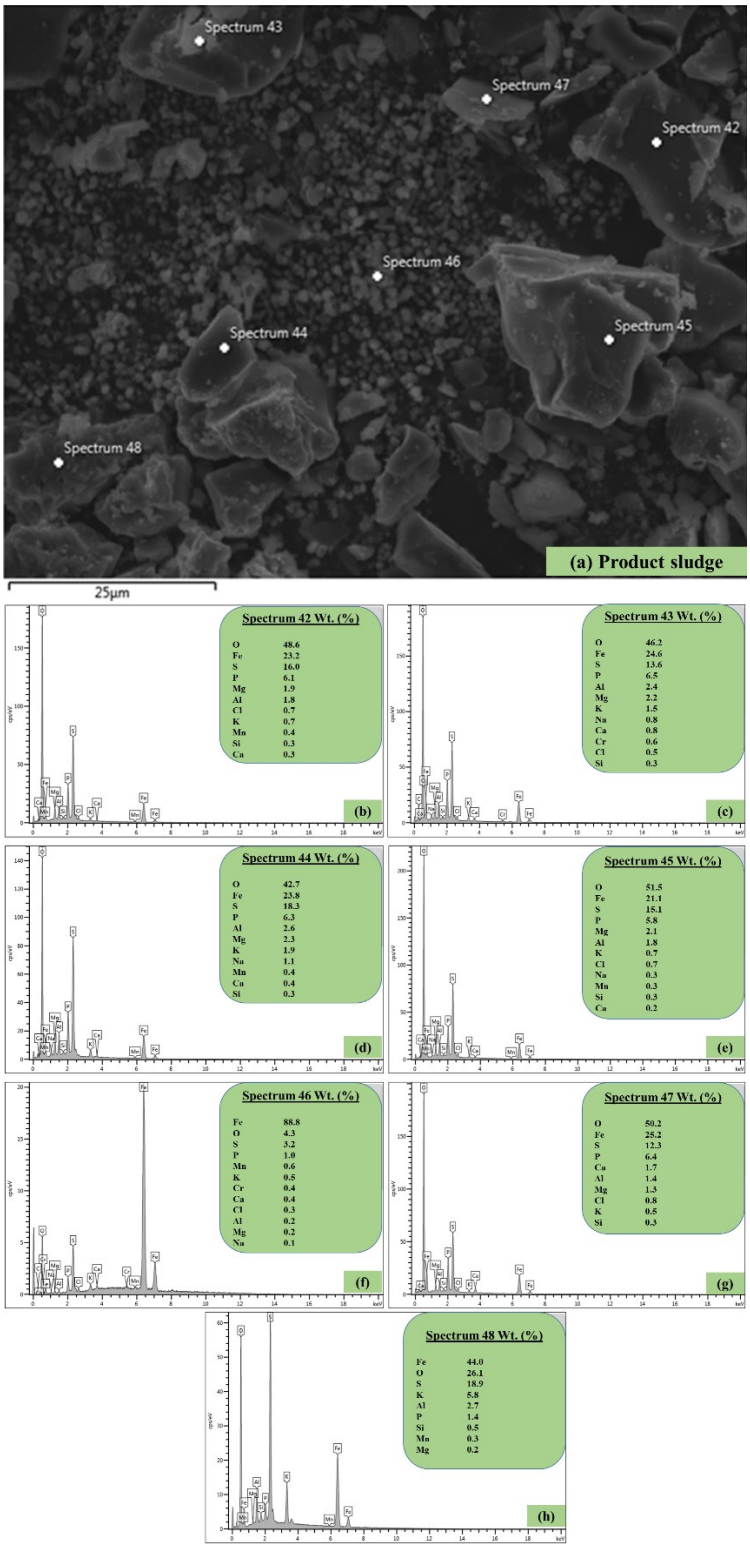
463 **Figure 8:** (a) The FE-SEM image product sludge and EDS elemental mapping for O (b), S (c), K

464 (d), Fe (e), P (f), Cl (g), Al (h), Mn (i), Si (j), Mg (k), Ca (l), Na (m), Cu (n), and Cr (o).

The elemental mapping confirmed the existence of O, S, K, Fe, P, Cl, Al, Mn, Si, Mg, Ca, Na, Cu and Cr in the sludge matrix (**Figure 8**). These elements were also identified in the sum peaks presented in **Figure 7**. The existence of these elements further support that the co-treatment of AMD and MWW can attenuate contaminants from both matrices, since the product sludge contains key elements from both of these matrices. Therefore, results suggest that the co-treatment of AMD and MWW can act as a passive treatment method for the AMD, while the MWW also enjoys some benefits of the co-treatment process, primarily due to P attenuation.

3.5.5 Spot analysis using HR-SEM-EDS

To further corroborate the results of the elemental composition, EDS spot-analysis was employed. The morphological properties and the spot-analysis with elemental distribution of the product sludge are shown in **Figure 9**.



477

478 **Figure 9 (a-h):** The SEM-EDS showing: (a) the spot analysis image for the product sludge, and

479 (b) – (h) the relevant EDS spectra.

Specifically, O, Fe, and S were identified as the main elements, while similarly to the elemental composition analysis (**Figure 8**) lower concentrations of P, Mg, Al, and K, along with traces of Ca, Si, Cl, and Na were identified in the product sludge (**Figure 9**). The FE-SEM results corroborate the estimates of the PHREEQC geochemical model, which largely emphasised the formation of K-jarosite, oxy-hydroxides, and oxy-hydrosulphates. These results are also in agreement with the FTIR and the EDS results . Furthermore, it appears that the product sludge comprises different sizes of morphological properties for boulders therein, but these have the same elemental composition. The obtained results further confirm that the interaction of AMD with MWW lead to the attenuation of the main contaminants from both matrices and the synthesis and precipitation of these minerals to the product sludge.

4 Conclusions and recommendations

The findings from this study suggest that the co-treatment of acid mine drainage (AMD) and municipal wastewater (MWW) is feasible, yet not promising for real-world applications due to the large MWW volume compare to the AMD volume. The efficacy of the process is primarily governed by dilution, which increases the pH of the AMD-MWW matrix, along with other mechanisms such as adsorption, co-adsorption, complexation, crystallization, co-precipitation, and precipitation. These mechanisms play a critical role in the attenuation of contaminants from these wastewater effluents. In detail, low AMD:MWW ratios, i.e., AMD is diluted into a higher MWW volumes, were found to improve co-treatment efficiency, with the optimal AMD:MWW ratio being 1:7. The optimum contact time, i.e., mixing duration, was 15 min (mixing speed 250 rpm), following by 30 min settling. The reaction kinetics were observed to be independent of temperature, hence the process will most probably not be affected by winter and summer temperature variations. Advanced analytical techniques (i.e., FTIR and FE-SEM-EDS)

confirmed the presence of O, Al, Fe, S, Mn, P, K, Ca and Mg as main elements in the product sludge, i.e., the sludge that is product after co-treatment. The sludge morphology was spherical, having a homogenous surface at different examined nano-scaled magnifications. The particles shapes were the same in different magnifications.

The PHREEQC model suggested that Fe-species were removed as Goethite, Hematite, Maghemite, magnetite, Jarosite (ss, K, Na, and H) and copper-based minerals, while Al was removed as Alunite and Jurbanite. Furthermore, Al and Fe were also precipitated as iron and aluminium (oxy)-hydroxides. Phosphates were removed as Pb, Mn, Al and Fe mineral phases. Ca and SO_4^{2-}were removed as gypsum, whilst Pb, Fe, Al were removed as hydroxyl sulphate minerals. Chemical species were observed to exist as oxyanions, monovalent, divalent, and trivalent ions, and as well as different complexes. In light of the above, the viability of co-treating AMD with MWW at industrial scale appear not to be practical considering the required volumes of MWW to AMD and their respective capacity and location. The product sludge was also highly mineralized and complex, thus making the recovery of the synthesized minerals challenging. Future research should focus on pre-treatment techniques, but more importantly on controlling the pH of the AMD-MWW matrix, e.g., by NaOH addition, as a mean to reduce the high MWW volumes. Finally, due to AMD's high iron content the Fenton's reagent can maximize the co-treatment efficiency.

Acknowledgement

The authors would like to thank the Magalies Water and the University of South Africa for supporting this project. Furthermore, the staff from the municipal wastewater treatment house

524 and mining houses are duly acknowledged for their support with sampling and access to the
525 facilities. Technicians who assisted with the analysis are duly acknowledged as well.

References

[1] Park, I., Tabelin, C.B., Jeon, S., Li, X., Seno, K., Ito, M., Hiroyoshi, N., A review of recent strategies for acid mine drainage prevention and mine tailings recycling. *Chemosphere*, 219, 588-606, 2019.

[2] Mavhungu, A., Foteinis, S., Mbaya, R., Masindi, V., Kortidis, I., Mpenyana-Monyatsi, L., Chatzisymeon, E., Environmental sustainability of municipal wastewater treatment through struvite precipitation: Influence of operational parameters. *Journal of Cleaner Production*, 124856, 2020.

[3] Mavhungu, A., Masindi, V., Foteinis, S., Mbaya, R., Tekere, M., Kortidis, I., Chatzisymeon, E., Advocating circular economy in wastewater treatment: Struvite formation and drinking water reclamation from real municipal effluents. *Journal of Environmental Chemical Engineering*, 103957, 2020.

[4] Masindi, V., Chatzisymeon, E., Kortidis, I., Foteinis, S., Assessing the sustainability of acid mine drainage (AMD) treatment in South Africa. *Science of the Total Environment*, 635, 793-802, 2018.

[5] Masindi, V., Akinwekomi, V., Maree, J.P., Muedi, K.L., Comparison of mine water neutralisation efficiencies of different alkaline generating agents. *Journal of Environmental Chemical Engineering*, 5, 3903-3913, 2017.

[6] Kefeni, K.K., Msagati, T.A.M., Mamba, B.B., Acid mine drainage: Prevention, treatment options, and resource recovery: A review. *Journal of Cleaner Production*, 151, 475-493, 2017.

[7] Tabelin, C.B., Veerawattananun, S., Ito, M., Hiroyoshi, N., Igarashi, T., Pyrite oxidation in the presence of hematite and alumina: I. Batch leaching experiments and kinetic modeling calculations. *Science of The Total Environment*, 580, 687-698, 2017.

[8] Rambabu, K., Banat, F., Pham, Q.M., Ho, S.-H., Ren, N.-q., Show, P.L., Biological Remediation of Acid Mine Drainage: Review of Past Trends and Current Outlook. *Environmental Science and Ecotechnology*, 100024, 2020.

[9] Naidu, G., Ryu, S., Thiruvenkatachari, R., Choi, Y., Jeong, S., Vigneswaran, S., A critical review on remediation, reuse, and resource recovery from acid mine drainage. *Environmental Pollution*, 247, 1110-1124, 2019.

[10] Talukdar, B., Kalita, H.K., Baishya, R.A., Basumatary, S., Sarma, D., Evaluation of genetic toxicity caused by acid mine drainage of coal mines on fish fauna of Simsang River, Garohills, Meghalaya, India. *Ecotoxicology and Environmental Safety*, 131, 65-71, 2016.

[11] Seo, J., Kwon, D., Yoon, T.H., Jung, J., Potential risks of the natural nanoparticles from the acid mine drainage and a novel approach for their toxicity assessment. *Toxicology and Environmental Health Sciences*, 2, 215-220, 2010.

[12] Dutta, M., Islam, N., Rabha, S., Narzary, B., Bordoloi, M., Saikia, D., Silva, L.F.O., Saikia, B.K., Acid mine drainage in an Indian high-sulfur coal mining area: Cytotoxicity assay and remediation study. *Journal of Hazardous Materials*, 389, 121851, 2020.

[13] Dsa, J.V., Johnson, K.S., Lopez, D., Kanuckel, C., Tumlinson, J., Residual toxicity of acid mine drainage-contaminated sediment to stream macroinvertebrates: Relative contribution of acidity vs. metals. *Water, Air, and Soil Pollution*, 194, 185-197, 2008.

[14] Da Silveira, F.Z., Defaveri, T.M., Ricken, C., Zocche, J.J., Pich, C.T., Toxicity and genotoxicity evaluation of acid mine drainage treatment using Artemia sp. and geophagus brasiliensis as bioindicators, in: 26th Annual Meetings of the American Society of Mining and Reclamation and 11th Billings Land Reclamation Symposium 2009, 2009, pp. 1704-1721.

[15] Masindi, V., Osman, M.S., Shingwenyana, R., Valorization of acid mine drainage (AMD): A simplified approach to reclaim drinking water and synthesize valuable minerals - Pilot study. *Journal of Environmental Chemical Engineering*, 7, 103082, 2019.

[16] Mavhungu, A., Mbaya, R., Masindi, V., Foteinis, S., Muedi, K.L., Kortidis, I., Chatzisymeon, E., Wastewater treatment valorisation by simultaneously removing and recovering phosphate and ammonia from municipal effluents using a mechano-thermo activated magnesite technology. *Journal of Environmental Management*, 250, 109493, 2019.
[17] Yang, C., Nan, J., Yu, H., Li, J., Embedded reservoir and constructed wetland for drinking water source protection: Effects on nutrient removal and phytoplankton succession. *Journal of Environmental Sciences*, 87, 260-271, 2020.
[18] Peng, L., Dai, H., Wu, Y., Peng, Y., Lu, X., A comprehensive review of phosphorus recovery from wastewater by crystallization processes. *Chemosphere*, 197, 768-781, 2018.
[19] Ekama, G.A., 4.14 - Biological Nutrient Removal A2 - Wilderer, Peter, in: *Treatise on Water Science*, Elsevier, Oxford, 2011, pp. 409-526.
[20] Oehmen, A., Lemos, P.C., Carvalho, G., Yuan, Z., Keller, J., Blackall, L.L., Reis, M.A.M., Advances in enhanced biological phosphorus removal: From micro to macro scale. *Water Research*, 41, 2271-2300, 2007.
[21] Abel-Denee, M., Abbott, T., Eskicioglu, C., Using mass struvite precipitation to remove recalcitrant nutrients and micropollutants from anaerobic digestion dewatering centrate. *Water Research*, 132, 292-300, 2018.
[22] Langmuir, D., Hall, P., Drever, J., *Environmental Geochemistry*, Prentice Hall, New Jersey, 1997.
[23] Ruihua, L., Lin, Z., Tao, T., Bo, L., Phosphorus removal performance of acid mine drainage from wastewater. *Journal of Hazardous Materials*, 190, 669-676, 2011.
[24] Vélez-Pérez, L.S., Ramirez-Nava, J., Hernández-Flores, G., Talavera-Mendoza, O., Escamilla-Alvarado, C., Poggi-Varaldo, H.M., Solorza-Feria, O., López-Díaz, J.A., Industrial acid mine drainage and municipal wastewater co-treatment by dual-chamber microbial fuel cells. *International Journal of Hydrogen Energy*, 2020.
[25] Strosnider, W.H.J., Nairn, R.W., Peer, R.A.M., Winfrey, B.K., Passive co-treatment of Zn-rich acid mine drainage and raw municipal wastewater. *Journal of Geochemical Exploration*, 125, 110-116, 2013.
[26] Strosnider, W.H., Winfrey, B.K., Nairn, R.W., Performance of an ecologically-engineered multistage acid mine drainage and municipal wastewater passive co-treatment system, in: 26th Annual Meetings of the American Society of Mining and Reclamation and 11th Billings Land Reclamation Symposium 2009, 2009, pp. 1391-1411.
[27] Hughes, T.A., Gray, N.F., Co-treatment of acid mine drainage with municipal wastewater: Performance evaluation. *Environmental Science and Pollution Research*, 20, 7863-7877, 2013.
[28] Strosnider, W.H., Winfrey, B.K., Nairn, R.W., Biochemical oxygen demand and nutrient processing in a novel multi-stage raw municipal wastewater and acid mine drainage passive co-treatment system. *Water Research*, 45, 1079-1086, 2011.
[29] Strosnider, W.H., Nairn, R.W., Effective passive treatment of high-strength acid mine drainage and raw municipal wastewater in Potosí, Bolivia using simple mutual incubations and limestone. *Journal of Geochemical Exploration*, 105, 34-42, 2010.
[30] Spellman, C.D., Tasker, T.L., Strosnider, W.H.J., Goodwill, J.E., Abatement of circumneutral mine drainage by Co-treatment with secondary municipal wastewater. *Journal of Environmental Management*, 271, 110982, 2020.
[31] Smyntek, P.M., Chastel, J., Peer, R.A.M., Anthony, E., McCloskey, J., Bach, E., Wagner, R.C., Bandstra, J.Z., Strosnider, W.H.J., Assessment of sulphate and iron reduction rates during reactor start-up for passive anaerobic co-treatment of acid mine drainage and sewage. *Geochemistry: Exploration, Environment, Analysis*, 18, 76-84, 2018.
[32] Wei, X., Viadero, R.C., Bhojappa, S., Phosphorus removal by acid mine drainage sludge from secondary effluents of municipal wastewater treatment plants. *Water Research*, 42, 3275-3284, 2008.

[33] Muedi, K.L., Brink, H.G., Masindi, V., Maree, J.P., Effective removal of arsenate from wastewater using aluminium enriched ferric oxide-hydroxide recovered from authentic acid mine drainage. *Journal of Hazardous Materials*, 414, 125491, 2021.
[34] Sibrell, P.L., Montgomery, G.A., Ritenour, K.L., Tucker, T.W., Removal of phosphorus from agricultural wastewaters using adsorption media prepared from acid mine drainage sludge. *Water Research*, 43, 2240-2250, 2009.
[35] Deng, D., Lin, L.S., Two-stage combined treatment of acid mine drainage and municipal wastewater. *Water Science and Technology*, 67, 1000-1007, 2013.
[36] Spellman, C., Strosnider, W., Tasker, T., Potential Implications of Acid Mine Drainage and Wastewater Co-treatment on Solids Handling: A Review. *Journal of Environmental Engineering*, 146, 2020.
[37] Masindi, V., A novel technology for neutralizing acidity and attenuating toxic chemical species from acid mine drainage using cryptocrystalline magnesite tailings. *Journal of Water Process Engineering*, 10, 67-77, 2016.
[38] Rose, C., Parker, A., Jefferson, B., Cartmell, E., The Characterization of Feces and Urine: A Review of the Literature to Inform Advanced Treatment Technology. *Critical Reviews in Environmental Science and Technology*, 45, 1827-1879, 2015.
[39] Sheoran, V., Sheoran, A.S., Choudhary, R.P., Biogeochemistry of acid mine drainage formation: A review, in: *Mine Drainage and Related Problems*, 2011, pp. 119-154.
[40] Amos, R.T., Blowes, D.W., Bailey, B.L., Sego, D.C., Smith, L., Ritchie, A.I.M., Waste-rock hydrogeology and geochemistry. *Applied Geochemistry*, 57, 140-156, 2015.
[41] Simate, G.S., Ndlovu, S., Acid mine drainage: Challenges and opportunities. *Journal of Environmental Chemical Engineering*, 2, 1785-1803, 2014.
[42] WHO, *Guidelines for drinking-water quality: fourth edition incorporating first addendum*, 4th ed + 1st add ed., World Health Organization, Geneva, 2017.
[43] EPA, Water Quality Standards Handbook, in: Chapter 3: Water Quality Criteria. EPA-823-B-17-001, EPA Office of Water, Office of Science and Technology, Washington, DC,https://www.epa.gov/sites/production/files/2014-10/documents/handbook-chapter3.pdf, 2017.
[44] SABS, South African National Standard (SANS), in: Drinking water - Part 2: Application of SANS 241-1 2015.
[45] Jadhav, D.A., Ghosh Ray, S., Ghangrekar, M.M., Third generation in bio-electrochemical system research – A systematic review on mechanisms for recovery of valuable by-products from wastewater. *Renewable and Sustainable Energy Reviews*, 76, 1022-1031, 2017.
[46] Masindi, V., Gitari, W.M., Ngulube, T., Kinetics and equilibrium studies for removal of fluoride from underground water using cryptocrystalline magnesite. *Journal of Water Reuse and Desalination*, 5, 282-292, 2015.
[47] Masindi, V., Ndiritu, J.G., Maree, J.P., Fractional and step-wise recovery of chemical species from acid mine drainage using calcined cryptocrystalline magnesite nano-sheets: An experimental and geochemical modelling approach. *Journal of Environmental Chemical Engineering*, 6, 1634-1650, 2018.
[48] Winfrey, B.K., Strosnider, W.H., Nairn, R.W., Strevett, K.A., Highly effective reduction of fecal indicator bacteria counts in an ecologically engineered municipal wastewater and acid mine drainage passive co-treatment system. *Ecological Engineering*, 36, 1620-1626, 2010.
[49] Strosnider, W.H.J., Winfrey, B.K., Peer, R.A.M., Nairn, R.W., Passive co-treatment of acid mine drainage and sewage: Anaerobic incubation reveals a regeneration technique and further treatment possibilities. *Ecological Engineering*, 61, Part A, 268-273, 2013.
[50] Strosnider, W.H., Winfrey, B.K., Nairn, R.W., Alkalinity Generation in a Novel Multi-stage High-strength Acid Mine Drainage and Municipal Wastewater Passive Co-treatment System. *Mine Water and the Environment*, 30, 47-53, 2011.

[51] Foteinis, S., Chatzisymeon, E., 4 - Heterogeneous photocatalysis for water purification, in: R. Boukherroub, S.B. Ogale, N. Robertson (Eds.) *Nanostructured Photocatalysts*, Elsevier, 2020, pp. 75-97.
[52] Lopes, F.A., dos Santos Menezes, J.C.S., Schneider, I.A.H., Acid mine drainage as source of iron for the treatment of sewage by coagulation and Fenton's reaction, in: A.F.C.W. Thomas R. Rüde (Ed.) "11th International Mine Water Association Congress – Mine Water – Managing the Challenges", *International mine water association (IMWA)*, Aachen, Germany, 2011, pp. 1-4.
[53] Tony, M.A., Lin, L.-S., Iron recovery from acid mine drainage sludge as Fenton source for municipal wastewater treatment. *International Journal of Environmental Analytical Chemistry*, 1-16, 2020.
[54] Tabelin, C.B., Corpuz, R.D., Igarashi, T., Villacorte-Tabelin, M., Alorro, R.D., Yoo, K., Raval, S., Ito, M., Hiroyoshi, N., Acid mine drainage formation and arsenic mobility under strongly acidic conditions: Importance of soluble phases, iron oxyhydroxides/oxides and nature of oxidation layer on pyrite. *Journal of Hazardous Materials*, 399, 122844, 2020.
[55] Magagane, N., Masindi, V., Ramakokovhu, M.M., Shongwe, M.B., Muedi, K.L., Facile thermal activation of non-reactive cryptocrystalline magnesite and its application on the treatment of acid mine drainage. *Journal of Environmental Management*, 236, 499-509, 2019.
[56] Akinwekomi, V., Maree, J.P., Masindi, V., Zvinowanda, C., Osman, M.S., Foteinis, S., Mpenyana-Monyatsi, L., Chatzisymeon, E., Beneficiation of acid mine drainage (AMD): A viable option for the synthesis of goethite, hematite, magnetite, and gypsum – Gearing towards a circular economy concept. *Minerals Engineering*, 148, 106204, 2020.